Design of Hybrid Magnet IPM Machine for Traction Applications

Satoshi Ghiba
Energy Department "Galileo Ferraris"
Politecnico di Torino
Turin, Italy
satoshi.ghiba@studenti.polito.it

Rishabh Raj
Electric Driveline Department
Volvo Cars Corporation
Gothenburg, Sweden
rishabh.raj@volvocars.com

Shayan Halder
Electric Driveline Department
Volvo Cars Corporation
Gothenburg, Sweden
shayan.halder@volvocars.com

Kim Bergsro
Electric Driveline Department
Volvo Cars Corporation
Gothenburg, Sweden
kim.bergsro@volvocars.com

Simone Ferrari
Energy Department "Galileo Ferraris"
Politecnico di Torino
Turin, Italy
simone.ferrari@polito.it

Gianmario Pellegrino
Energy Department "Galileo Ferraris"
Politecnico di Torino
Turin, Italy
gianmario.pellegrino@polito.it

***Abstract*—This work proposes a hybrid permanent magnet material based synchronous machine design, combining the advantages of rare-earth free iron nitride magnets with rare earth magnets. The primary goal of the work is to propose a solution for automotive applications for a passenger car vehicle, capable of reaching the required performance and withstanding active short-circuit events without significant irreversible demagnetization. The study also aims to minimize the content of expensive and climate intensive rare-earth permanent magnet. The proposed design has a reduction of 70% of the rare-earth materials content, without performance degradation. The cost and performance of the proposed design are compared to a benchmark machine with rare earth permanent magnets.**

***Index Terms*—iron nitride, hybrid permanent magnets, active short circuit, demagnetization, optimization.**

I. Introduction

The reliance of the automotive industry on rare earth elements, particularly Neodymium and Dysprosium, used in the production of high performance permanent magnets used in Interior Permanent Magnet Synchronous Machines (IPMSM) poses significant challenges. Some of these rare earth elements are relatively abundant on the planet, but their main problem comes from difficulties in their extraction. Furthermore, due to their non-uniform distribution, they are primarily controlled by a few countries, leading to price volatility and supply chain risks [1]. In addition, the environmental impact of their extraction raises sustainability concerns, pressing the industry to seek alternative solutions [2].

Several alternatives of electric machines have been considered to reduce the dependence of the industry on rare earths. For instance, Electrically Excited Synchronous Machines [3]–[6] can provide good performance without any use of these materials. However, this comes at the cost of an increase in the amount of copper used, potentially shifting the the environmental damage. Other solutions include Induction Machines [7], which are rare-earth-free but do not achieve the same performance of PMSMs. The work mentioned in [8]–[11] focuses on PMSMs that utilizes magnets materials like ferrite and iron-nitride (FeN) , that are obtained from materials which are more available and with lower environmental impact. However, these solutions are highly sensitive to demagnetization, particularly during an active short circuit (ASC) [8] event. Further, the work performed in [12]–[20] explored designs that take advantage of both rare-earth and non-rare-earth magnets, trying to leverage the advantages of both magnet materials. In all the above mentioned work, the transient three phase ASC has still not been investigated.

This work extends that presented in [10] and [11] by proposing a design method for sizing hybrid magnet material based interior permanent magnet machine (hybrid-IPM) which combines Iron Nitride and NdFeB magnets. The demagnetization during an active short-circuit is identified as a key problem, and the design is therefore optimized to provide the required performance even after an ASC event on the machine side. Furthermore, an attempt is made to minimize the cost and environmental impact of the magnets used in a electric machine. Finally, a design is proposed and compared to a benchmark PMSM with NdFeB magnets by comparing the cost, climate impact, and the average efficiency with a sample vehicle on the WLTC drive cycle.

II. Machine Design Approach in Finite Element Simulations

A. Design Topology

In this subsection, two Interior Permanent Magnet (IPM) machines are compared to find the best starting design for a hybrid-IPM. This machine uses a mix of both rare earth (RE) viz. NdFeB magnet and rare-earth-free (REF) viz. FeN magnets. In each of the two cases, the stator geometry and the machine windings are kept identical. The analysis mainly focuses on the rotor geometry to achieve a specified machine performance.

In particular, two different configurations for the placement of RE and REF magnets are considered: Topology A where the two types of permanent magnet (PM) are magnetically in parallel, and Topology B where they are in a series-parallel setup [17], as shown in Fig.1. Both topologies are characterized by the same mass of each type of PM used. Moreover, a thorough sensitivity analysis has been conducted which lead to the analysis that the most successful way to increase the demagnetization performance of the magnets is to increase their width and to move them further away from the rotor outer diameter.

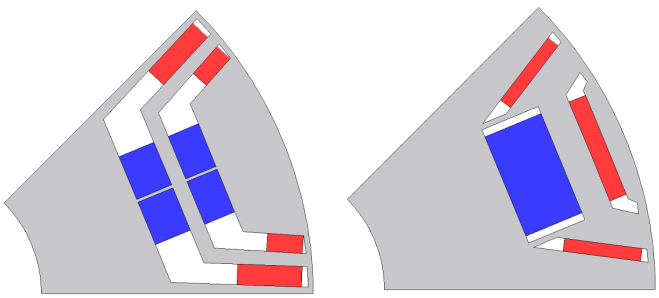

Fig. 1. Machine Topologies with RE magnets in red and REF magnets in blue: (a) Topology A, (b) Topology B.

Therefore, the optimal way to maximize the utilization of such a hybrid-magnets configuration is to have those with the lower coercive field aligned to d-axis. In the next subsections, the demagnetization performance of the two configurations are summarized. Further, the better performing topology is optimized using a set of objective functions. The topologies and the design analysis is performed in a JMAG [21], a finite element analysis (FEA) tool.

B. ASC and Demagnetization Evaluation

The ASC can be considered an important and critical fault condition, particularly for electrical machines which make use of REF permanent magnets. This condition can be used for evaluating the risk of irreversible demagnetization. This can be done by introducing the concept of *demagnetization ratio* as

$$d = \left(1 - \frac{B_r}{B_{r,0}\left(\Theta\right)}\right) \cdot 100 \qquad (1)$$

where d is the demagnetization ratio, B_r is the residual flux density of a particular load point, and $B_{r,0}\left(\Theta\right)$ is the residual flux density of the non-demagnetized magnet at temperature Θ. It is important to note that the given analytical equation can produce values greater than 100% when the numerator becomes negative, indicating a magnetization of the magnet in the opposite direction to the initial magnetization. An in-built functionality from FEA software to compute demagnetization compared to non-demagnetized state also can be adopted for the same purpose.

One of the widely used methodologies to evaluate the peak transient ASC event utilizes the extended flux maps of the electric machine, either by FEA, or from experimental data, and then solves the analytical equations. Another approach would be evaluating the peak transient ASC in lossless conditions. The second approach is faster due to lower number of FEA computations, but also overestimates the peak current value since the losses in machine would dampen the ASC peak transient current value [22]. SyR-e [23], the open-source FEA software also used in this work, allows to implement both of the previously stated methodologies, but the flux map based analysis approach is opted for better accuracy. During this analysis, the iron losses are not considered and the speed of the rotor is kept constant. In any case, the worst case scenario should be obtained starting at base speed and maximum braking torque since the produced negative d-axis current would be the highest [24], [25].

In this work, the transient ASC is evaluated at the lowest temperature, which is identified as the worst case condition for this hybrid-IPM considering the nature of RE magnets. In general, ASC and demagnetization analysis are done at higher temperatures, since the coercivity of RE magnet is lower. In the case of hybrid-IPM, REF magnets are highly stable in temperature, while the RE magnets have higher flux remanence which in turn produces higher ASC currents.

C. FEA Results and Comparison

For topologies A and B, the results are obtained with procedural steps. First, the torque is evaluated at the Base speed with the maximum phase current, and the current angle estimated from the Maximum Torque per Ampere (MTPA) trajectory. Then, the expected worst case ASC is obtained with SyR-e at the Maximum Torque and Base speed. Then, the currents are applied on the machine, and the demagnetization is evaluated using (1). The FEA model intentionally utilizes a reversible model for the RE magnet, so that the difference in performance can be attributed only to the irreversible demagnetization of the REF magnet. Finally, the torque is evaluated with the identical speed and current vector for the same machine but without the REF magnet; this simulation is used as a dummy simulation, representing the complete REF magnet demagnetization. The results are reported in Table I.

TABLE I
DEMAGNETIZATION MAXIMUM CURRENT

	Topology A	**Topology B**
Peak negative d-axis current (A_{pk})	1816	1570
Average demagnetization after ASC (%)	77	56
Torque before ASC (p.u.)	1.589	1.347
Torque after ASC (p.u.)	0.913	1.225
Torque without REF magnet (p.u.)	0.657	1.076

The torque requirements are met with both topologies, and the average demagnetization can be used as a figure of merit for the comparison. The conclusion that can be reported from this analysis is that with topology B the RE magnet witnesses an increase in the demagnetization performance during a transient worst case ASC event. This is due to the presence of the higher coercivity RE magnet that acts as a ”barrier”. In this way, the load line of the iron nitride is shifted, and the REF magnet is subjected to a lower demagnetizing field. Furthermore, the peak torque is less affected by this ASC event with this rotor topology, as a 9% torque reduction is witnessed, while with topology A the torque reduction after a worst scenario ASC event is around 42%.

III. Machine Design Optimization

A. Optimization Strategy

Topology B is identified as a the better design in terms of resistance to worst case ASC event; a detailed design approach is implemented with this choice of topology. The selected topology is further analysed and enhanced to find a better fit of magnet configuration. This resulted in keeping the RE PMs magnetically in series with the REF one of the inner flux-barrier, leading to a design that resembles a double inset-mount hybrid-IPM (DIM-hybrid-IPM) machine as shown in Fig.2. This DIM-hybrid-IPM is further used as an initial design for a multi-objective genetic algorithm based optimization study.

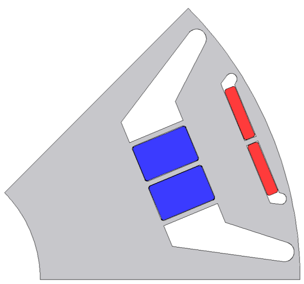

Fig. 2. Initial topology of the optimization.

The procedure reported in this work is applicable to any possible hybrid-IPM topology. The approach includes the minimization of the machine losses which in general is used by machine designers for an efficient machine design. An additional step is the identification of the worst case transient peak currents during an ASC event. Moreover, the baseline geometry has the additional features of including an air gap between the magnet and the rotor steel laminates of 0.1 mm, and fillets on the magnet edge. The added air gap is a realistic representation of manufacturing tolerances for insertion of magnets in the pockets. Instead, the fillets on the edges are used for minimizing the risk of demagnetization. The inclusion of the manufacturing tolerance related air gap in the rotor leads to an increase of the equivalent air gap that the flux encounters. This leads to an increase in the equivalent reluctance seen by the magnet flux which increases the slope of the load line, as well as the risk of demagnetization. Therefore, this needs to be taken into account for a realistic and practical machine design.

The adopted optimization process aims to obtain a design that can achieve the target performance after a worst case ASC event. The current amplitude and angle are kept constant for every evaluation and the value used is decided the optimization process. In particular, this is set with an initial MTPA based calculation. This simplification helps to reduce the computational complexity, since the demagnetizing currents are heavily dependant on the pre-fault condition.

The evaluation for each optimization candidate comprises of two steps:

1) The machine is demagnetized with a negative d-axis current. This is a simplification of the actual possible worst case ASC event, since a non-zero q-axis current will influence the flux penetration in the rotor and thereby the demagnetization in the machine. The amplitude of the ASC current is the same for each candidate, and is obtained by implementing the initial geometry in SyR-e based built-in algorithm, and by following the previously explained procedure, at the start of this subsection. This value is chosen as the initial maximum current value from a pre-fault condition of 565 A$_{pk}$.
2) The machine is then supplied with the maximum current and the approximated current angle, evaluating the torque post a possible worst case ASC event.

The geometry of the machine is parameterized on the dimensions of the flux barriers and ribs in rotor, except for the width of the iron ribs which are set as constant.

The objectives and constraints used in this optimization are reported in (2).

$$\begin{aligned} \min_{x_1,x_2,x_3,x_4} \quad & \frac{x_1}{f_1} + \frac{x_2}{f_2} + \frac{x_3}{f_3} + \frac{x_4}{f_4} \\ \text{s.t.} \quad & T_{postASC} > 1.076 \end{aligned} \tag{2}$$

Where x_1 is the PM Cost, x_2 the PM EPS, x_3 the losses in A, and x_4 the losses in B. In particular, $f1$, $f2$, $f3$, and $f4$ are factors which were respectively obtained from a FEM simulation for the initial geometry (Fig.2) and represent the PM Cost, the PM EPS, the losses in A, and the losses in B.

In particular the torque after an ASC event is set as a requirement. Then, following the environmental priority strategy method (EPS), the damage costs for emissions and use of natural resources measured in ELU (Environmental Load Units) can be minimized [26]. The data used for this procedure is proprietary and is not reported in this work. Furthermore, after defining a sample vehicle, the total machine losses in the two operating points, which fall under most the common WLTC cycle points, are also minimized. The two operating points are given in Table II and are utilized to improve the WLTC efficiency of the machine.

TABLE II
Optimized WLTC points

	Speed [rpm]	Torque [Nm]
Point A	11593	22.6
Point B	7596	15

B. Optimization Results

In this work, the general rule followed for setting up the optimization is that for a geometry which has n parameters, the optimization should have at least $10n$ the number of generations, and at least $n+1$ cases [10].

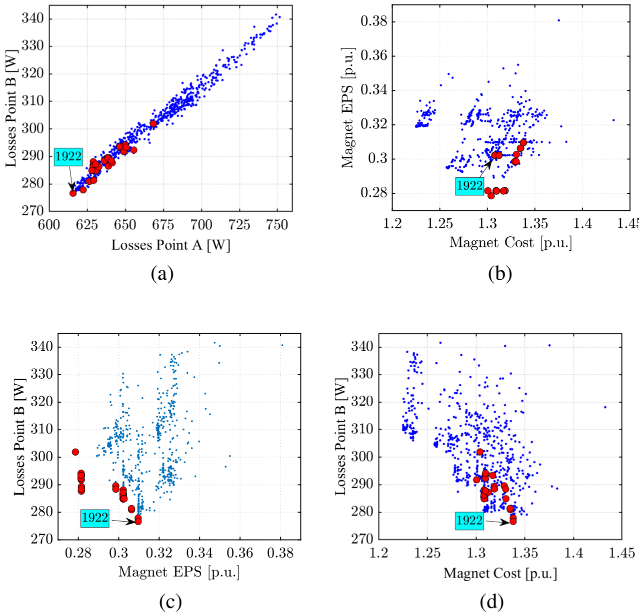

Fig. 3. Pareto front of the optimization with filtered solutions (a) total machine losses at point A vs point B, (b) magnet EPS vs magnet cost, (c) total machine losses at point B vs magnet EPS, (d) total machine losses at point B vs magnet cost.

In this work, the model is parameterized with 13 variables. Following the previous indications, the optimization is run with 14 cases for 140 generations. These numbers can be increased for better performance, at the cost of the computational time. The resulting geometries are filtered to obtain only the designs meeting the torque performance requirements. Fig.3 shows the Pareto front plots obtained from the performed optimization study. The red dots illustrates the optimal solution, with each highlighting different trade-offs between competing objectives. Fig.3a depicts the effect on the total losses during

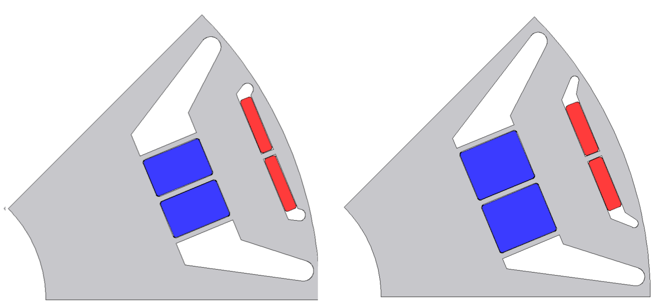

(a) (b)

Fig. 4. Machine geometry: (a) during the start of optimization, (b) the optimized design.

the optimization, while the second Pareto plot in Fig.3b shows the magnet cost and EPS. Further, Fig.3c and Fig.3c show the Pareto front for the losses in point B as a function of the EPS and of the cost of the magnet respectively. The results of this optimization study indicates that for satisfying the objective functions, a reduction in cost and EPS is required. This in turn results in an increase in the total losses of the machine, and consequently a reduction in efficiency. In this work, the selected solution is the one that minimizes the losses, as an increase in efficiency would also results in better range, and consequently the profit on the vehicle level. Fig.4 shows the starting and the final optimized rotor geometry.

IV. Performance Verification

A. Normal Operation

The performance characteristics of the best design from the optimization is compared to a fully RE magnet based benchmark IPM machine. Table III reports the main characteristics for the benchmark and for the hybrid-IPM. The two machines have same winding configuration, with a different active length and stator diameter. The hybrid-IPM manages to reach fairly close to the torque and power requirements, even when considering the reduction from manufacturing effects and the effect of a worst case ASC event. However, the torque density of the benchmark remains higher. Moreover, given its lower torque at high speed, a higher gear ratio is chosen for the proposed machine. As tabulated, the hybrid-IPM reduces the amount of RE magnet by 73% compared to the benchmark-IPM but the overall magnet mass in the hybrid-IPM is increased by 37% comparatively. The WLTC efficiency has been optimized by minimizing the losses in the two operating points reported in Table II. The efficiency maps of the proposed machine and for the benchmark machine are shown in Fig.5. Note that these efficiencies were obtained by applying correction factors to account for the manufacturing effects on the steel. The average efficiency during the WLTC drive cycle for the hybrid-IPM is 95.08 %, while the efficiency for the benchmark machine is about 94.87%.

TABLE III
Benchmark and Hybrid PM characteristics

Ratings	Benchmark	Proposed
Maximum Power (p.u.)	1	0.814
Maximum Torque (p.u.)	1	0.978
Mass (p.u.)	1	1.078
Torque density (p.u.)	1	0.908
Gear ratio (p.u)	1	1.327
RE magnet mass (p.u.)	1	0.27
REF magnet mass (kg)	N.A	1.30
Outer stator diameter (mm)	1	0.978
Supply Voltage (p.u.)	1	1
Maximum Phase Current (p.u.)	1	1
Stack length (mm)	1	1.149

B. Demagnetization Performance

The procedure for evaluating the worst case ASC event has been re-evaluated for the selected solution. The resulting current in the (i_d, i_q) plane is reported in Fig.6. Table IV reports the maximum negative d-axis current, as well as the performance before and after an ASC event. The torque value obtained with this ASC-demag evaluation does not consider manufacturing effect reductions and thus a raw value from

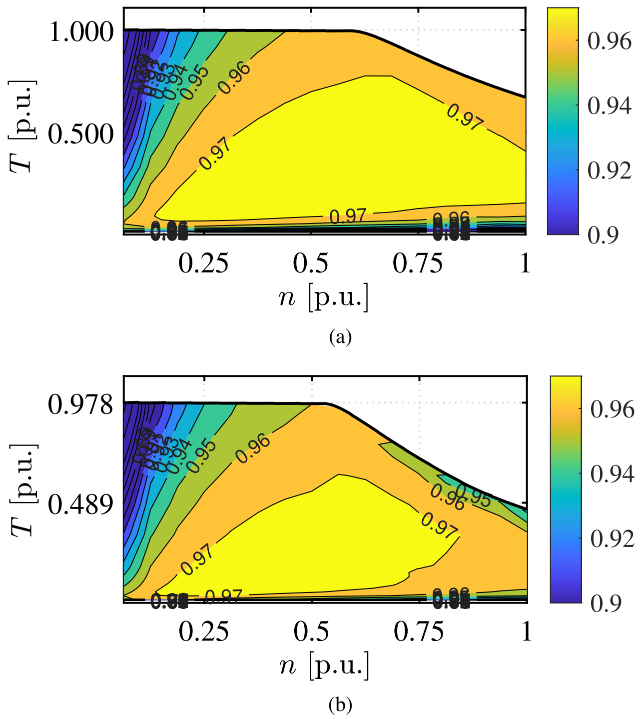

Fig. 5. Efficiency on the torque-speed map for : (a) benchmark-IPM, (b) hybrid-IPM.

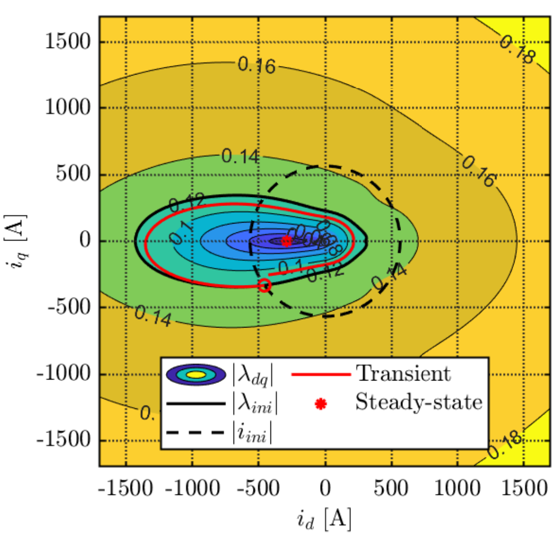

Fig. 6. Transient short circuit of case number 1922.

FEA results is reported for simplicity. As a result, after an ASC event, the torque of the machine is reduced by around 3.7%.

C. Environmental impact and cost

The environmental impact of the design is considered in two separate steps. First, the environmental priority strategy is used, which is measured in ELU and considers the impact of every kilogram of material used. The results show that the final design has a 14.8% lower EPS compared to the benchmark, even considering the higher total mass of the machine compared to benchmark. This is determined by the much lower EPS of the REF magnets compared to the RE based alternatives. Then, the climate impact is considered by adding a premium on the calculation cost of the machine for each kilogram of CO_2 emissions generated by the manufacturing of the machine. Since the cost of RE material is very volatile, Fig.7 shows the cost increase of the hybrid-IPM

TABLE IV
FINAL DESIGN DEMAGNETIZATION PERFORMANCE

Attributes	**Value**
Peak negative d-axis current during ASC (A_{pk})	1350
Average demagnetization after ASC (%)	14.8
Torque before ASC (p.u.)	1.11
Torque after ASC (p.u.)	1.073

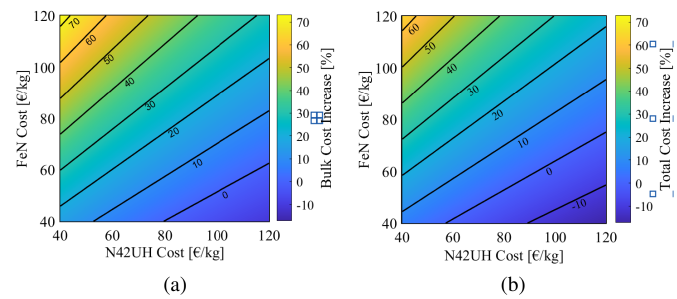

Fig. 7. Machine cost increase (in %) compared to the benchmark, as a function of REF and RE magnet's cost in €/kg: (a) bulk cost, (b) total cost.

compared to the benchmark-IPM as a function of the cost of the magnets. The break even lines are reported for the bulk cost, which considers the cost of the materials, and for the total cost, which considers the cost of the mass increase compared to the machine and the influence of the increase in WLTC performance.

V. CONCLUSIONS

In this work, a hybrid-IPM based design is proposed, consisting of RE and REF magnets. In particular, the ASC event is considered as critical, given the lower coercive nature of REF magnets [27]. The work focuses on optimizing the rotor side geometry for generating better performances, without optimizing stator geometry and windings configurations. The two machine design topologies based on design of rotor iron ribs and the corresponding magnet placement are investigated and compared. Topology B is chosen as the better solution for reaching the requirements after an ASC event. Further, a detailed optimization is performed on a DIM-hybrid-IPM machine, and an evaluation is conducted on the selected solution to obtain its demagnetization performance after a worst case ASC event. The proposed machine has 73% lower RE magnet content when compared to a benchmark RE based IPM machine with the similar performance. The total magnet mass is higher compared to benchmark-IPM, but the EPS is lower due to the presence of REF magnets. The proposed machine is also characterized for the average efficiency over a WLTC drive cycle considering a reference vehicle. The proposed machine is as efficient as the reference as far as the WLTC drive cycle is concerned, but has the advantage of a lower ELU, making it a comparatively sustainable solution.

REFERENCES

[1] N. M. I. Center, "Rare earths statistics and information," United States Geological Survey, Tech. Rep., 2023. [Online]. Available: https://www.usgs.gov/centers/national-minerals-information-center/rare-earths-statistics-and-information

[2] S. R. Golroudbary, I. Makarava, A. Kraslawski, and E. Repo, "Global environmental cost of using rare earth elements in green energy technologies," *Science of The Total Environment*, vol. 832, p. 155022, 2022. [Online]. Available: https://www.sciencedirect.com/science/article/pii/S0048969722021155

[3] I. Kokubo and K. Kiyota, "Investigation of efficiency enhancement of a wound-field flux switching motor by the synchronous reluctance motor drive," in *2023 26th International Conference on Electrical Machines and Systems (ICEMS)*, 2023, pp. 1254–1259.

[4] Z. Q. Zhu and X. Liu, "Novel stator electrically field excited synchronous machines without rare-earth magnet," in *2014 Ninth International Conference on Ecological Vehicles and Renewable Energies (EVER)*, 2014, pp. 1–13.

[5] G. Petrelli, S. Nuzzo, D. Barater, T. Zou, G. Franceschini, and C. Gerada, "Preliminary sensitivity analysis and optimisation of a wound field synchronous motor for traction applications," in *2023 AEIT International Conference on Electrical and Electronic Technologies for Automotive (AEIT AUTOMOTIVE)*, 2023, pp. 1–6.

[6] F. I. Wibisono and J. Asama, "Wound field synchronous motor using a non-salient pole rotor with distributed winding," in *2023 IEEE Energy Conversion Congress and Exposition (ECCE)*, 2023, pp. 4030–4033.

[7] T.-K. Kim, J.-H. Kim, J.-H. Kim, G.-C. Kim, J.-H. Lee, C.-G. Yeo, and S.-Y. Jung, "Experimental comparison of induction motor and ipmsm with identical stator," in *2023 IEEE Energy Conversion Congress and Exposition (ECCE)*, 2023, pp. 4208–4215.

[8] A. Vagati, B. Boazzo, P. Guglielmi, and G. Pellegrino, "Design of ferrite-assisted synchronous reluctance machines robust toward demagnetization," *IEEE Transactions on Industry Applications*, vol. 50, no. 3, pp. 1768–1779, 2014.

[9] G. Dilevrano, P. Ragazzo, S. Ferrari, and G. Pellegrino, "Comparative design of ferrite- and ndfeb-pmsms using the (x,b) design plane," in *2023 IEEE International Electric Machines Drives Conference (IEMDC)*, 2023, pp. 1–7.

[10] G. S. L'Abbate, "Design of ipm machines for traction using rare-earth-free iron-nitride magnets," Politecnico di Torino, Tech. Rep., 2023.

[11] A. Al-Qarni and A. EL-Refaie, "Design and optimization of high-performance rare-earth free interior permanent magnet motors for electric vehicles enabled by iron nitride magnets," in *2023 IEEE Energy Conversion Congress and Exposition (ECCE)*, 2023, pp. 4082–4089.

[12] R. Wilson, P. Kumar, and A. El-Refaie, "Minimization of rare-earth permanent magnets and demagnetization risk in pm-assisted synchronous reluctance motor with blended magnets," in *2023 IEEE Energy Conversion Congress and Exposition (ECCE)*, 2023, pp. 4257–4264.

[13] Y. Ji, Y. Li, and Q. Lu, "Investigation of a novel hybrid less-rare-earth consequent-pole interior permanent magnet machine with asymmetric rotor," in *2023 26th International Conference on Electrical Machines and Systems (ICEMS)*, 2023, pp. 5354–5359.

[14] P. Kumar, R. Wilson, T. Chowdhury, and A. EL-Refaie, "Multi-objective design optimization and comparison of 2-layer versus 3-layer pm-assisted synchronous reluctance machines using a blend of rare-earth and rare-earth-free magnets," in *2023 IEEE Energy Conversion Congress and Exposition (ECCE)*, 2023, pp. 3930–3937.

[15] M. K. Ghosh, B. Grainger, S. McElhinny, R. Brody, J. Cui, A. Sherman, and P. Ohodnicki, "Multiphysics design and optimization of a rare-earth free, manganese bismuth based, surface mounted permanent magnet machine," in *2023 IEEE Transportation Electrification Conference Expo (ITEC)*, 2023, pp. 1–7.

[16] W. Cui, L. Ren, J. Zhou, and Q. Zhang, "A new ipmsm with hybrid rotor structure for electrical vehicle with reduced magnet loss," *IEEE Transactions on Magnetics*, vol. 58, no. 2, pp. 1–6, 2022.

[17] B. Poudel, E. Amiri, P. Rastgoufard, and B. Mirafzal, "Toward less rare-earth permanent magnet in electric machines: A review," *IEEE Transactions on Magnetics*, vol. 57, no. 9, pp. 1–19, 2021.

[18] B. Raghuraman, S. Nategh, N. Sidiropoulos, L. Petersson, and A. Boglietti, "Sustainability aspects of electrical machines for e-mobility applications part i: A design with reduced rare-earth elements," in *IECON 2021 – 47th Annual Conference of the IEEE Industrial Electronics Society*, 2021, pp. 1–6.

[19] Q. Ma, A. El-Refaie, and B. Lequesne, "Low-cost interior permanent magnet machine with multiple magnet types," *IEEE Transactions on Industry Applications*, vol. 56, no. 2, pp. 1452–1463, 2020.

[20] Z. S. Du and T. A. Lipo, "Cost-effective high torque density bi-magnet machines utilizing rare earth and ferrite permanent magnets," *IEEE Transactions on Energy Conversion*, vol. 35, no. 3, pp. 1577–1584, 2020.

[21] J. International, "Jmag-designer." [Online]. Available: https://www.jmag-international.com/products/jmag-designer/

[22] S. Ferrari, G. Dilevrano, P. Ragazzo, P. Pescetto, and G. Pellegrino, "Fast determination of transient short-circuit current of pm synchronous machines via magnetostatic flux maps," *IEEE Transactions on Industry Applications*, vol. 59, no. 4, pp. 4000–4009, 2023.

[23] S. Ferrari and G. Pellegrino, "SyR-e: Synchronous Reluctance (machines) - evolution." [Online]. Available: www.github.com/SyR-e/syre_public

[24] S. T. Lee, "Demagnetization study of an interior permanent magnet synchronous machine considering transient peak 3 phase short circuit current," in *2017 IEEE Energy Conversion Congress and Exposition (ECCE)*, 2017, pp. 4694–4698.

[25] G. Choi and T. M. Jahns, "Demagnetization characteristics of permanent magnet synchronous machines," in *IECON 2014 - 40th Annual Conference of the IEEE Industrial Electronics Society*, 2014, pp. 469–475.

[26] S. L. C. Center, "Environmental priority strategies in product design (eps)." [Online]. Available: https://www.lifecyclecenter.se/projects/environmental-priority-strategies-in-product-design-eps/

[27] R. Wilson, P. Kumar, and A. El-Refaie, "Minimization of rare-earth permanent magnets and demagnetization risk in pm-assisted synchronous reluctance motor with blended magnets," in *2023 IEEE Energy Conversion Congress and Exposition (ECCE)*, 2023, pp. 4257–4264.